Ge22As20Se58 glass ultrafast laser inscribed waveguides for mid-IR integrated optics

Morris, James M.; Mackenzie, Mark D.; Petersen, Christian Rosenberg; Demetriou, Giorgos; Kar, Ajoy K.; Bang, Ole; Bookey, Henry T.

Published in:
Optical Materials Express

Link to article, DOI:
10.1364/OME.8.001001

Publication date:
2018

Document Version
Publisher's PDF, also known as Version of record

Research Article | Vol. 8, No. 4 | 1 Apr 2018 | OPTICAL MATERIALS EXPRESS 1001
Optical Materials EXPRESS

$Ge_{22}As_{20}Se_{58}$ glass ultrafast laser inscribed waveguides for mid-IR integrated optics

JAMES M. MORRIS,[1,2,*] MARK D. MACKENZIE,[2] CHRISTIAN R. PETERSEN,[3] GIORGOS DEMETRIOU,[2] AJOY K. KAR,[2] OLE BANG,[3] AND HENRY T. BOOKEY[1]

[1]*Fraunhofer Centre for Applied Photonics, Technology and Innovation Centre, 99 George Street, Glasgow G1 1RD, UK*
[2]*Institute of Photonics and Quantum Sciences, David Brewster Building, Heriot-Watt University, Edinburgh, EH14 4AS, UK*
[3]*DTU Fotonik, Department of Photonics Engineering, Technical University of Denmark, DK-2800 Kgs. Lyngby, Denmark*
**jm510@hw.ac.uk*

Abstract: Ultrafast laser inscription has been used to produce channel waveguides in $Ge_{22}As_{20}Se_{58}$ glass (GASIR-1, Umicore N.V). The mode field diameter and waveguide losses at 2.94 μm were measured along with the waveguide dispersion in the 1 to 4.5 μm range, which is used to estimate the zero-dispersion wavelength. Z-scan measurements of bulk samples have also been performed to determine the nonlinear refractive index. Finally, mid-IR supercontinuum generation has been shown when pumping the waveguides with femtosecond pulses centered at 4.6 μm. Supercontinuum spanning approximately 4 μm from 2.5 to 6.5 μm was measured which, to the best of the authors' knowledge, represents the broadest and the deepest IR supercontinuum from an ultrafast laser inscribed waveguide to date. This work, combined with the long wavelength transmission of GASIR-1 up to 15 μm, paves the way for realizing further ultrafast laser inscribed waveguide devices in GASIR-1 for mid-IR integrated optics applications.

OCIS codes: (130.2755) Glass waveguides; (130.3060) Infrared; (160.4330) Nonlinear optical materials.

References and links

1. D. W. Hewak, "Chalcogenide glasses for photonics device applications," in *Photonic Glasses and Glass-Ceramics,* G. S. Murugan, ed. (Research Signpost, 2010).
2. B. J. Eggleton, B. Luther-Davies, and K. Richardson, "Chalcogenide photonics," Nat. Photonics **5**(3), 141–148 (2011).
3. A. Ródenas, G. Martin, B. Arezki, N. Psaila, G. Jose, A. Jha, L. Labadie, P. Kern, A. Kar, and R. Thomson, "Three-dimensional mid-infrared photonic circuits in chalcogenide glass," Opt. Lett. **37**(3), 392–394 (2012).
4. C. R. Petersen, N. Prtljaga, M. Farries, J. Ward, B. Napier, G. R. Lloyd, J. Nallala, N. Stone, and O. Bang, "Mid-infrared multispectral tissue imaging using a chalcogenide fiber supercontinuum source," Opt. Lett., early posting (2018).
5. N. D. Psaila, R. R. Thomson, H. T. Bookey, S. Shen, N. Chiodo, R. Osellame, G. Cerullo, A. Jha, and A. K. Kar, "Supercontinuum generation in an ultrafast laser inscribed chalcogenide glass waveguide," Opt. Express **15**(24), 15776–15781 (2007).
6. J. McCarthy, H. Bookey, S. Beecher, R. Lamb, I. Elder, and A. K. Kar, "Spectrally tailored mid-infrared super-continuum generation in a buried waveguide spanning 1750 nm to 5000 nm for atmospheric transmission," Appl. Phys. Lett. **103**(15), 151103 (2013).
7. M. R. Karim, B. M. Rahman, and G. P. Agrawal, "Mid-infrared supercontinuum generation using dispersion-engineered $Ge_{11.5}As_{24}Se_{64.5}$ chalcogenide channel waveguide," Opt. Express **23**(5), 6903–6914 (2015).
8. M. R. Karim and B. M. A. Rahman, "Ultra-broadband mid-infrared supercontinuum generation using chalcogenide rib waveguide," Opt. Quantum Electron. **48**(3), 174 (2016).
9. Y. Yu, X. Gai, P. Ma, D. Y. Choi, Z. Y. Yang, R. P. Wang, S. Debbarma, S. J. Madden, and B. Luther-Davies, "A broadband, quasi-continuous, mid-infrared supercontinuum generated in a chalcogenide glass waveguide," Laser Photonics Rev. **8**(5), 792–798 (2014).

#319549 https://doi.org/10.1364/OME.8.001001
Journal © 2018 Received 1 Feb 2018; revised 10 Mar 2018; accepted 10 Mar 2018; published 22 Mar 2018

Optical Materials EXPRESS

10. Y. Yu, X. Gai, P. Ma, K. Vu, Z. Yang, R. Wang, D. Y. Choi, S. Madden, and B. Luther-Davies, "Experimental demonstration of linearly polarized 2-10 μm supercontinuum generation in a chalcogenide rib waveguide," Opt. Lett. **41**(5), 958–961 (2016).
11. H. Lin, Z. Luo, T. Gu, C. Kimerling Lionel, K. Wada, A. Agarwal, and J. Hu, "Mid-infrared integrated photonics on silicon: a perspective," in *Nanophotonics,* (2017), p. 393.
12. P. Mitchell, G. Brown, R. R. Thomson, N. Psaila, and A. Kar, "57 Channel (19x3) Spatial Multiplexer Fabricated using Direct Laser Inscription," in *Optical Fiber Communication Conference*, OSA Technical Digest (online) (Optical Society of America, 2014), M3K.5.
13. T. A. Birks, I. Gris-Sánchez, S. Yerolatsitis, S. G. Leon-Saval, and R. R. Thomson, "The photonic lantern," Adv. Opt. Photonics **7**(2), 107 (2015).
14. G. Demetriou, D. W. Hewak, A. Ravagli, C. Craig, and A. Kar, "Nonlinear refractive index of ultrafast laser inscribed waveguides in gallium lanthanum sulphide," Appl. Opt. **56**(19), 5407–5411 (2017).
15. J. A. Frantz, L. B. Shaw, J. S. Sanghera, and I. D. Aggarwal, "Waveguide amplifiers in sputtered films of Er3+-doped gallium lanthanum sulfide glass," Opt. Express **14**(5), 1797–1803 (2006).
16. J. Morris, N. K. Stevenson, H. T. Bookey, A. K. Kar, C. T. A. Brown, J. M. Hopkins, M. D. Dawson, and A. A. Lagatsky, "1.9 μm waveguide laser fabricated by ultrafast laser inscription in Tm:Lu_2O_3ceramic," Opt. Express **25**(13), 14910–14917 (2017).
17. R. Mary, D. Choudhury, and A. K. Kar, "Applications of Fiber Lasers for the Development of Compact Photonic Devices," IEEE J. Sel. Top. Quant. **20**(5), 72–84 (2014).
18. M. Sheik-Bahae, A. A. Said, T. H. Wei, D. J. Hagan, and E. W. Van Stryland, "Sensitive measurement of optical nonlinearities using a single beam," IEEE J. Quantum Electron. **26**(4), 760–769 (1990).
19. T. Wang, X. Gai, W. Wei, R. Wang, Z. Yang, X. Shen, S. Madden, and B. Luther-Davies, "Systematic z-scan measurements of the third order nonlinearity of chalcogenide glasses," Opt. Mater. Express **4**(5), 1011–1022 (2014).
20. G. Demetriou, J.-P. Bérubé, R. Vallée, Y. Messaddeq, C. R. Petersen, D. Jain, O. Bang, C. Craig, D. W. Hewak, and A. K. Kar, "Refractive index and dispersion control of ultrafast laser inscribed waveguides in gallium lanthanum sulphide for near and mid-infrared applications," Opt. Express **24**(6), 6350–6358 (2016).
21. C. R. Petersen, U. Møller, I. Kubat, B. Zhou, S. Dupont, J. Ramsay, T. Benson, S. Sujecki, N. Abdel-Moneim, Z. Tang, D. Furniss, A. Seddon, and O. Bang, "Mid-infrared supercontinuum covering the 1.4–13.3 μm molecular fingerprint region using ultra-high NA chalcogenide step-index fibre," Nat. Photonics **8**(11), 830–834 (2014).

1. Introduction

The Mid-Infrared (mid-IR) spectral region (2 – 20 μm) is of increasing importance in a large array of photonics applications, such as: medical diagnosis, spectroscopy, sensing and astronomy [1–4]. Many of these applications also benefit from utilizing an integrated optics platform due to its inherent advantages in size, robustness, scalability and alignment free operation over free space setups. This growing interest necessitates the development and demonstration of photonic devices compatible with integrated optics platforms in host materials suitable for the mid-IR; one such group of these materials are chalcogenide glasses.

Chalcogenide glasses contain one or more of the chalcogen elements sulphur (S), selenium (Se) or tellurium (Te) as their main component and are ideally suited to mid-IR applications because they can transmit light up to ~20 μm. Chalcogenide materials also exhibit glass forming behavior across a large range of compositional variations which allows for broad tuning of the resulting glass transmittance, linear (n_0) and nonlinear (n_2) indices, and mechanical properties. Intrinsically, chalcogenide glasses have a large nonlinear response due to the polarizability of the heavier chalcogen elements they contain and the covalent bonding they exhibit. Chalcogenide glasses can have n_2 values up to ~1000 larger than that of fused silica and are therefore suitable for applications in compact sources of mid-IR supercontinuum [5, 6].

Recently, there have been several theoretical and experimental demonstrations of channel waveguides in Ge-As-Se glasses for mid-IR supercontinuum generation. Karim *et al.* [7] presented a numerical study of air clad $Ge_{11.5}As_{24}Se_{64.5}$ ridge waveguides on MgF_2 reporting a supercontinuum spanning from 1.8 to 7.7 μm when pumping with a peak power of 500 W at a wavelength of 3.1 μm. Subsequently, in a further theoretical study, Karim *et al.* [8] show a 1.8 to 8 μm supercontinuum could be output from $Ge_{11.5}As_{24}Se_{64.5}$ rib waveguides on MgF_2 using 85 fs pulses centered at 3.1 μm with a peak power of 500 W. Yu *et al.* [9] have reported an experimental demonstration of a 1.8 to >7.5 μm supercontinuum from a $Ge_{11.5}As_{24}Se_{64.5}$ glass rib waveguide on a $Ge_{11.5}As_{24}S_{64.5}$ substrate by pumping the waveguide with ~320 fs

Optical Materials EXPRESS

pulses at 4 μm and a peak power of ~3kW. In their work the long wavelength edge of the supercontinuum was limited by absorption in the protective fluoropolymer coating applied to the waveguides. Yu *et al.* [10] have also presented experimental results showing a linearly polarized supercontinuum spanning 2 to 10 μm produced by pumping a buried rib waveguide, consisting of a $Ge_{11.5}As_{24}Se_{64.5}$ core and a $Ge_{11.5}As_{24}S_{64.5}$ cladding, with 330 fs pulses centered at 4184 nm and 4.5 kW peak power. These theoretical studies and experimental demonstrations have all employed waveguides produced using 2D planar fabrication techniques which allow for high index contrast and therefore tight confinement, which is advantageous for many integrated optics applications in the mid-IR [11]. These techniques do however have disadvantages such as process complexity and limited scope for vertical stacking of components.

For this work we utilize Ultrafast Laser Inscription (ULI) as our fabrication method as it is an established technique for producing channel waveguides in transparent dielectrics that can be used to create complex integrated optics devices such as photonic lanterns, couplers and fanouts [12–14]. In comparison with planar fabrication techniques used to create chalcogenide channel waveguides for integrated optics, for instance photolithography and etching [9] or lift-off techniques [15], ULI has many advantages, such as three dimensional design freedom, the possibility for rapid prototyping and single step fabrication. ULI utilizes ultrashort laser pulses (hundreds of femtoseconds to few picoseconds) to induce permanent refractive index change in a transparent dielectric. Depending on the material response to ultrashort pulses both refractive index increase and decrease (Type I and Type II, respectively) can be demonstrated along with control of the magnitude of the induced change. This gives flexibility in the type of waveguides that can be written and allows for tailoring of properties, such as the guided mode size.

In this study, we report the successful fabrication of mid-IR channel waveguides in GASIR-1 utilizing the ULI method. The waveguide losses, $1/e^2$ mode field diameter (MFD) values and dispersion parameters are determined. We also present measurements of the nonlinear material response of GASIR-1. Mid-IR supercontinuum generation has been demonstrated when pumping the channel waveguides with femtosecond pulses centered at 4.6 μm. A supercontinuum spanning approximately 4 μm from 2.5 to 6.5 μm was measured, which to the best of the authors knowledge is the broadest and deepest IR supercontinuum from a ULI fabricated waveguide to date. GASIR-1 was selected for this study as it is a commercially available material (Umicore N.V.) with high optical quality and transmission range from 1 - 15 μm which makes it an ideal candidate for mid-IR integrated optics applications.

2. Waveguide fabrication and characterization

A study of the response of GASIR-1 to ULI processing methods was undertaken using a mode-locked Yb-doped fiber laser (IMRA μ-Jewel D400) which emits 360 fs pulses with a central wavelength of 1045 nm and a pulse repetition rate of 500 kHz. The laser pulse train was passed through power and polarization control optics to set the inscribing pulse energy and circular polarization. Finally, the pulse train was focused using a 0.4 NA aspheric lens to give a focal spot diameter of approximately 1.8 μm.

GASIR-1 samples were mounted on air bearing stages and passed through the focus of the aspheric lens using the transverse writing geometry to write lines of modified material across a range of inscribing beam pulse energies to study the effect the parameter sweep has on the material modification. It has been shown in other studies that transitions from Type I to Type II guiding are possible above a pulse energy threshold [16]. Modification lines were written at a depth of ~250 μm below the sample surface to avoid surface ablation during writing and with consideration of the working distance of the objective and the sample thickness. After each inscription run the sample was removed and the sample end facets imaged using a microscope with transmission illumination to characterize the inscribed regions. This allows

Optical Materials EXPRESS

for both the determination of the cross section of the modified tracks and a rough assessment of the type of refractive index change induced by checking for light guiding. An end facet image showing the results of one such pulse energy parameter sweep is shown in Fig. 1.

From the pulse energy sweep studies, it was found that for these writing conditions only Type I index change could be produced. At the higher pulse energies larger Type I regions extending up towards the sample surface were produced, i.e. in the pre-focal section of the focused beam. These studies also showed for incident pulse energies of 12 nJ the modified region was approximately rectangular with height (extent in the z direction as defined in Fig. 1) equal to the confocal parameter (z_c) of the focused beam in the samples, calculated using:

$$z_c = 2\frac{n_0 M^2 \lambda}{\pi NA^2} \quad (1)$$

For GASIR-1 which has a n_0 of ~2.54 at the inscribing wavelength and given the M^2 value for the inscription laser of 1.2, this gives a modification region height of ~13 µm for 12 nJ pulses. Careful control of the inscribing pulse energy in a few nJ range around 12 nJ allowed for adjusting the height of the modification lines from ~10 to ~15 µm whilst maintaining the rectangular cross section.

With the ULI parameters established for controllable Type I modification, waveguides were fabricated using the multi-scan writing technique at a depth of ~250 µm from the sample surface. The multi-scan technique was used so that waveguide width (extent in the x direction as defined in Fig. 1) could be controlled in a deterministic manner that is decoupled from changes in the waveguide height [17]. This allowed for the fabrication of arrays of waveguides with different core sizes. For this work, a waveguide array was fabricated containing 7 waveguides with core widths ranging from 2 to 8 µm and core heights of 15 µm (which are referred to as WG1-7 in order of ascending core width and shown in Fig. 1) Waveguide core dimensions were chosen based on mid-IR ULI waveguides produced in other chalcogenide glasses [6]. Once inscribed, the waveguide end facets were ground back and re-polished to remove any defects caused by clipping of the writing beam at the sample edges, creating waveguides of 8 mm in length.

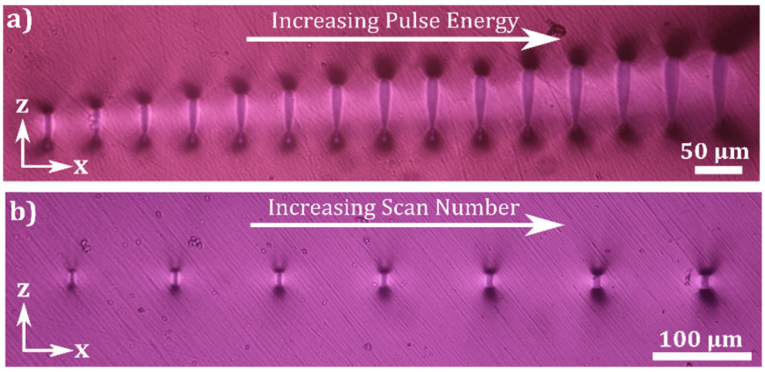

Fig. 1. Transmission microscope images showing the resulting material modification from two fabrication parameter sweeps. a) single line scan results for increasing pulse energies from 34 to 90 nJ. b) The array of multi-scan waveguides used in this work. Written with identical laser parameters but increasing scan number to vary the waveguide core width. In both cases the inscription beam is incident from above.

Waveguide losses and MFD measurements were performed for each waveguide in the array by fixing the inscribed sample in a waveguide alignment workstation. An overview of the experimental setup is given in Fig. 2 along with the waveguide losses and $1/e^2$ MFD values for each waveguide. Light was coupled into and collected from the individual waveguides using a pair of 0.25 NA ZnSe objectives (Innovation photonics, antireflection

Optical Materials EXPRESS

coated for 2 - 12 µm). The collection objective was used to image the output facet directly onto the sensor of a mid-IR InSb camera (FLIR SC7000) or power meter for mode imaging and loss measurements, respectively. Input power measurements into the waveguides were taken by moving the power meter in front of the first objective. The signal laser used was a Er:YAG mid-IR laser emitting up to 1 W at 2.94 µm (Sheaumann 2.94 µm MirPac). All the stated waveguide losses account for Fresnel reflections at both the input and output facets and so consist of the contribution from coupling and propagation losses. The $1/e^2$ MFD values were calculated using a gaussian fit to the mode image formed on the InSb sensor with a scale factor determined by taking images of calibration targets mounted in place of the inscribed sample.

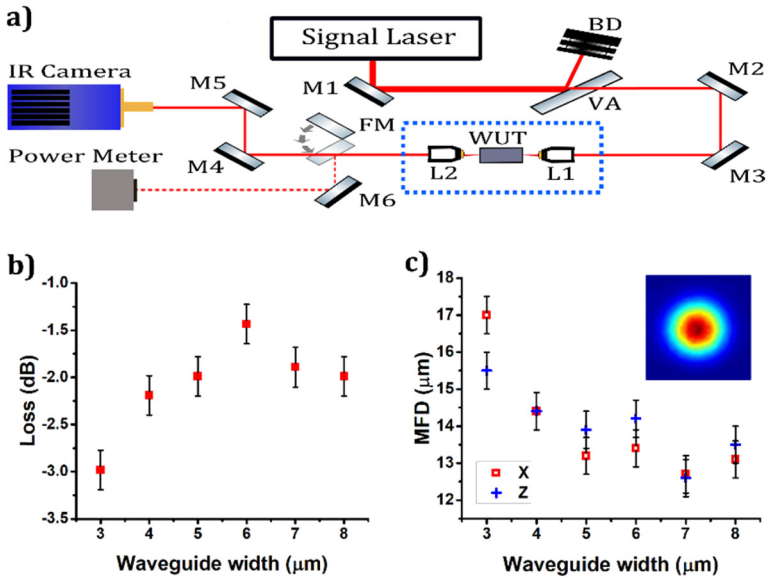

Fig. 2. Experimental setup for initial waveguide testing, waveguide losses and guided mode dimensions. a) Setup where: Mx, silver mirrors; VA, reflective variable ND filter; BD, beam dump; L1 and L2, BBAR-coated ZnSe objectives; WUT, waveguide under test; FM, flip mirror. Blue dotted box signifies components mounted on waveguide alignment workstation. b) Waveguide losses including coupling and propagation loss for WG2-7. c) Waveguide $1/e^2$ MFD measurements for x and z directions for WG2-7 with an insert showing the near field mode image of WG5.

It was found that WG1, which has the smallest core, offered poor confinement at the signal laser wavelength and so losses and MFDs could only be accurately determined for WG2 to WG7 which correspond to core widths of 3 to 8 µm. In this range, the waveguide MFDs were observed to decrease from an average value of 16.25 µm ± 0.5 µm to an average value of ~13 µm ± 0.5 µm. For WG2 the guided mode was slightly elliptical with the weak lateral confinement resulting in a larger MFD in the x direction, for the remaining waveguides the guided modes were observed to be circular to within the error in the measurement technique. WG2 to WG5 were observed to be single mode at 2.94 µm whereas first order modes could be excited in WG6 and WG7 with the input spot misaligned. The lowest loss measured was 1.4 dB ± 0.21 dB for WG5 which has a cross section of 6 by 15 µm and accounts for Fresnel loss. By making the conservative assumption that the lowest measured loss represents perfect coupling into WG5, i.e. no coupling losses from mode field mismatch, we can provide an upper estimate for the propagation loss of the waveguides of 1.75 dBcm^{-1} ± 0.26 dB cm^{-1}. The manufacturer provided attenuation coefficient for GASIR-1 at 3 µm is less than 0.01 cm^{-1} and so the origin of the propagation loss can be seen to be from the waveguide.

Optical Materials EXPRESS

3. Mid-IR Z-scans

Measurements of the n_2 of GASIR-1 were performed by means of the closed aperture Z-scan technique, described elsewhere [18], using 120 fs pulses output from a OPA (Spectra Physics OPA-800) pumped by a regeneratively amplified modelocked Ti:Sapphire laser operating at 1 kHz. The OPA output can be tuned from 1.1 to 1.6 μm for the signal and from 1.6 to 2.9 μm for the idler and therefore the idler output of the OPA can be used to investigate n_2 values into the mid-IR. To ensure a Gaussian spatial profile, as required by the theoretical fit used to determine n_2 in this work, the output of the OPA was first focused through a pinhole held in vacuum to remove any higher order spatial modes and recollimated before entering the Z-scan section of the setup. A pick off beam splitter was also placed in the collimated section of the beam path to divert approximately 8% of the beam onto a photodetector (New Focus 2033 or Thorlabs PDA30G-EC for 1.55 μm or 2 and 2. 5 μm measurements, respectively) which was used to compensate for laser power fluctuations. The OPA output was finally focused using an uncoated 20 cm focal length CaF_2 lens giving beam waists of 26, 28 and 32 μm for the 1.55, 2 and 2.5 μm beams, respectively. A 1 mm thick GASIR-1 sample was translated through the focus along the beam path whilst recording the far-field transmittance through an aperture using a second identical photodetector. The aperture was set to transmit 50% of the input beam without a sample in the beam path. This setup allowed for the recording of closed-aperture Z-scan traces at tunable Infrared wavelengths, as shown in Fig. 3, with measurements taken at 1.55, 2 and 2.5 μm. Extending n_2 measurements further into the mid-IR was limited by the stable tuning range of the OPA and sensitivity range of the photodetectors.

The closed aperture Z-scans were fitted using the empirical normalized Z-scan transmittance formula to determine the sign and magnitude of the n_2 for the sample [18]:

$$T_{cl}(z) = 1 + \frac{4x\Delta\phi_0(1-S)^{0.25}}{(1+x^2)(9+x^2)} \tag{2}$$

where x is the relative sample position given by $x = z/z_r$; z_r is the Rayleigh range of the focused beam given by $z_r = \pi\omega_0^2/\lambda$, with ω_0 the beam waist and λ the test wavelength; $\Delta\phi_0$ is the on axis time averaged phase change for spatially and temporally gaussian pulses given by $\Delta\phi_0 = 2\pi L n_2 I_0/(\lambda\sqrt{2})$, with L the sample length and I_0 the on axis peak intensity of the laser pulses.

The occurrence of any multiphoton absorption (MPA) was monitored using normalized plots of transmitted power with an open aperture, i.e. 100% transmittance in the absence of a sample, in order to ensure MPA was not affecting the measurements. The onset of MPA was observed to occur for pulse energies around 10 nJ at 1.55 and 2 μm and around 130 nJ at 2.5 μm. This is consistent with a change in MPA order from two to three photon absorption given the center wavelengths of the pulses. A UV-Vis transmission spectrometer (Lambda 950) was used to investigate this which showed that although the band edge of GASIR-1, defined by the absorption coefficient exceeding 10^4 m^{-1}, is in the region of 664 nm there is a long absorption tail with some residual linear absorption out beyond 1 μm.

A positive nonlinearity was observed as is evident from the shape of the Z-scan trace which indicates a nonlinear focusing of the beam by the sample. The magnitude of the n_2 was seen to monotonically decrease for increasing wavelengths, as is shown in Fig. 3. These n_2 values were validated by comparing the measured n_2 value at 1.55 μm to published literature. The value measured in this work of 5.5×10^{-18} $m^2/W \pm 15\%$ is in close agreement with the same glass composition in a recent large-scale Z-scan study of various chalcogenide glasses at 1.55 μm which was reported as 5.62×10^{-18} m^2/W [19].

Optical Materials EXPRESS

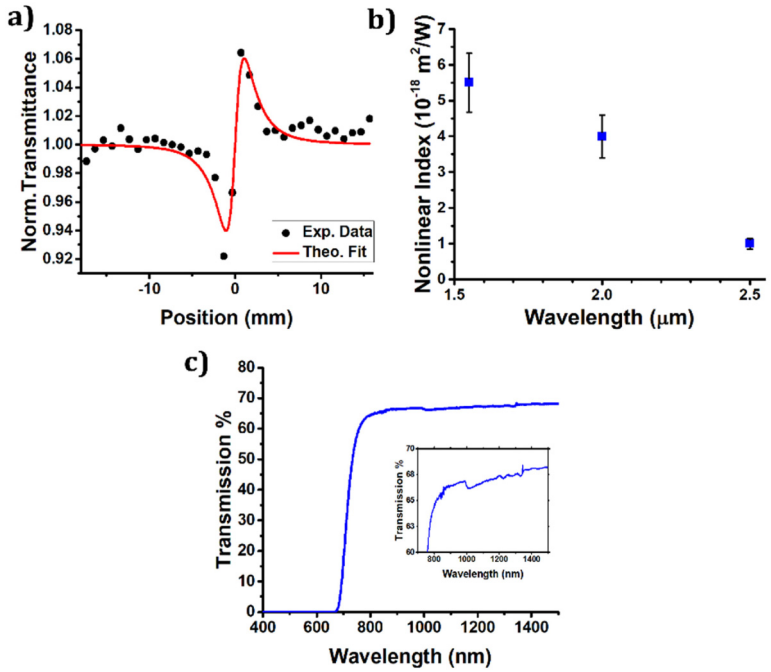

Fig. 3. Z-scan measurement and spectrometer results. a) Representative Z-scan trace taken using 10 nJ pulses centered at 2 μm with a linear aperture transmittance of 50% and fit using the closed aperture Z-scan formula. b) Plot of measured n_2 values vs wavelength including errors (± 15%). c) Transmission spectra showing band edge with a zoomed in view insert showing the absorption tail, includes Fresnel losses.

4. Waveguide dispersion

The dispersion of the waveguides was measured by white-light interferometry using a mid-IR supercontinuum source (NKT Photonics), a balanced Mach-Zehnder interferometer, and a scanning spectrometer (Spectro 320, Instrument Systems). A detailed description of the method is found in [20, 21]. Figure 4 shows the measured dispersion for four different waveguides.

For each waveguide four measurements were performed at different optical path delays yielding different interference patterns that resulted in slight variations in the fitted dispersion curve. For this reason, the dispersion curves in Fig. 4 represent the mean over these four measurements, with error bars indicating the variation in the fits. Because of the limited sampling the fits vary significantly near the edges of the spectrum, and especially at the short-wavelength edge where the dispersion slope is very steep. The inset zoomed in view on the long-wavelength edge of the measurement shows the variation at the long-wavelength edge more clearly together with an estimated zero-dispersion wavelength (ZDW) around 4.44 μm and 4.56 μm for WG1 and WG3, respectively. The measured dispersion was found to be almost the same for each waveguide despite the large geometric difference, which indicates that the dispersion is dominated by material dispersion and that the refractive index contrast is low. The measured dispersion of the larger WG5 and WG7 was limited on the long-wavelength side by the source and on the low-wavelength side below 1.7 μm side by interference from higher-order modes.

Optical Materials EXPRESS

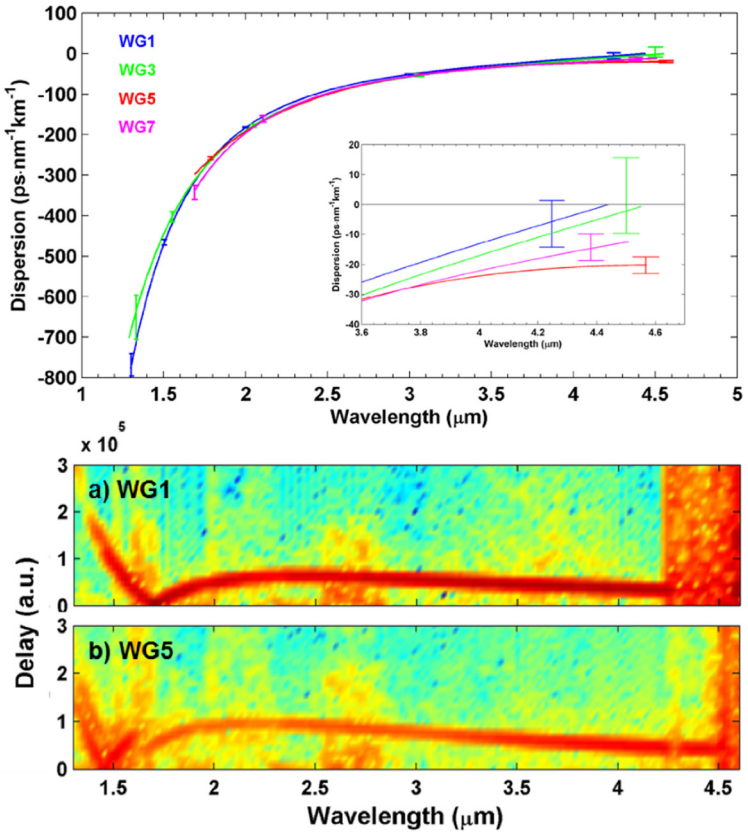

Fig. 4. Dispersion results and analysis. Top: Measured dispersion of different waveguides. The lines represent the mean of four measurements with error bars indicating measurement uncertainty. The insert shows a zoomed in view on the long-wavelength edge of the measurement, indicating a ZDW around 4.44 μm and 4.56 μm for WG1 and WG3, respectively. Bottom: Windowed Fourier transform analysis of interference spectra from a) WG1 and b) WG5, which demonstrates that WG5 exhibit multimode beating below 1.7 μm. In this particular example the higher-order mode is dominating at short wavelengths making it difficult to measure the dispersion in this region.

The presence of higher-order modes is also visualized in Fig. 4 through windowed Fourier transform spectrograms. The spectrograms translate the interference patterns into a delay curve, which result in a delay curve for each significant mode. The spectrograms show that WG1 exhibits only a single dominant mode, whereas two distinct traces are seen for WG5 below 1.7 μm. Moreover, the higher-order mode appears to dominate over the fundamental mode at shorter wavelengths making it difficult to measure the dispersion in this region.

Optical Materials EXPRESS

5. Waveguide supercontinuum generation

For supercontinuum generation, the waveguides were pumped by mid-IR femtosecond pulses produced by difference frequency generation (DFG) using a $AgGaS_2$ crystal. The DFG crystal is synchronously pumped by the signal and idler outputs of the aforementioned OPA in section 3. Residual signal and idler power was blocked by a long pass 2.5 μm filter. The difference frequency output was passed through a tunable MgF_2 half-wave plate and a BaF_2 wire grid polarizer for power and polarization control. A flip mirror was used to divert the beam onto a power meter for incident power measurements. Light was coupled into and collected from the individual waveguides using a pair of 0.25 NA ZnSe objectives (Innovation photonics, antireflection coated for 2 - 12 μm) or 20 mm focal length uncoated CaF_2 lenses (Thorlabs LA5315). The waveguide output was alternately imaged directly onto the sensor of a mid-IR InSb camera (FLIR SC7000) for alignment and to record the guided mode profiles or through a monochromator (Zolix Omni-λ300) to measure the output spectrum. The monochromator was used with a cryogenically cooled mercury cadmium telluride (MCT) detector (Zolix DMCT12) and a lock-in amplifier (Princeton Applied Research 5209) to measure the spectral power distribution of the supercontinuum. A 3.6 μm long pass filter was used to remove any higher order diffraction effects caused by the gratings in the monochromator. The experimental setup used and results are shown in Fig. 5.

Supercontinuum width was observed to increase with increasing waveguide core size. This is explained by better coupling of the input light through improved mode matching and a decreasing waveguide MFD which enhances nonlinear interactions. Furthermore, for the smaller waveguides longer wavelengths, as was the case for WG1 at 2.94 μm, are not well confined. The pump pulse wavelength was chosen to be centered at 4.6 μm as this is above the ZDW for the smaller waveguides and is also within the range of the InSb camera used for waveguide alignment. The largest waveguide, WG7, produced a supercontinuum spanning approximately 4 μm from 2.5 to 6.5 μm when pumped with 130 nJ pulses, corresponding to a peak power of ~1000 kW, coupled and collected using the CaF_2 lens set. To the authors knowledge, this represents the broadest and deepest IR supercontinuum from a ULI waveguide to date. Pumping with higher energy pulses did not improve the result which we attribute to the onset of MPA depleting the pulse. This is supported by the visible surface damage to the waveguide end facet that occurred when increasing the pulse energy further to around 300 nJ. The dispersion characterization of the larger WGs revealed that they exhibit normal dispersion at 4.6 μm and therefore supercontinuum generation occurred for a pump centered below the ZDW.

By measuring the pump spot size and waveguide MFDs for below threshold energy pulses at 4.6 μm we could identify that the ZnSe objectives provided the best mode matching and therefore lowest coupling loss into WG5. This allowed for an investigation of the threshold energy for the onset of spectral broadening in WG5 which was found to be at around 3 nJ of incident pulse energy, corresponding to a peak power of ~24 kW. Broader supercontinuum generation is predicted for pump pulses centered deeper into the mid-IR beyond the ZDW but the drop off in sensitivity of the InSb camera used for waveguide alignment in this work restricted the testing of above ZDW pumping for the larger waveguides.

Optical Materials EXPRESS

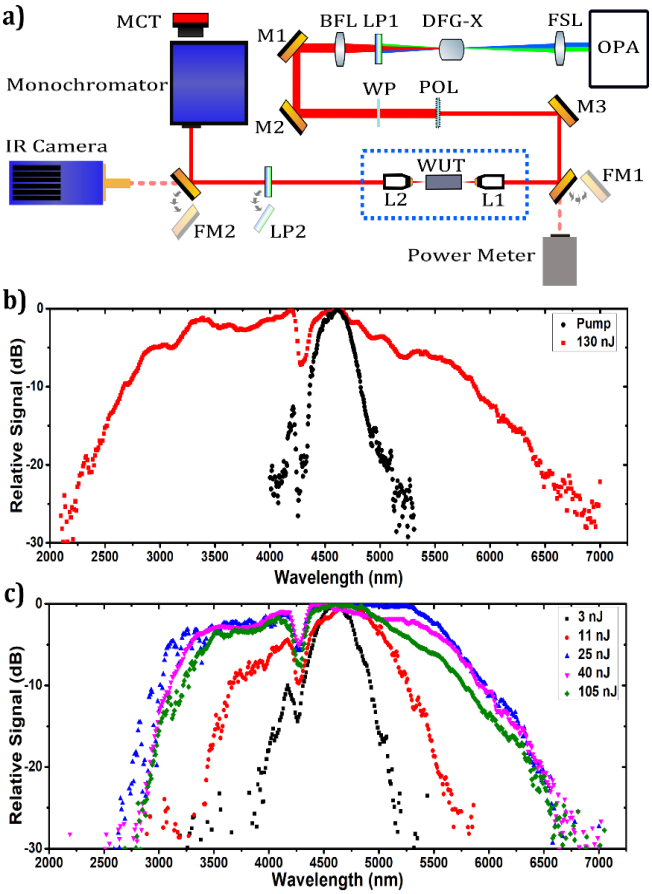

Fig. 5. Supercontinuum measurement setup and results. a) Setup where: Mx, gold mirrors; FSL, fused silica lens; DFG-X, DFG crystal; BFL, BaF_2 lens; LPx, long pass filters; WP, waveplate; POL, wire grid polarizer; FMx, flip mirrors; L1 and L2, BBAR-coated ZnSe objectives or uncoated CaF_2 lens; WUT, waveguide under test; MCT, MCT detector. Blue dotted box signifies components mounted on waveguide alignment workstation. b) Broadest supercontinuum measured spanning ~4 um at –20 dB points. Produced by pumping WG7 with 130 nJ pulses coupled and collected with CaF_2 lens set. Input pulse spectrum is also shown. c) Evolution of supercontinuum with input pump power for WG5 with ZnSe objective set. Broadening is seen from pulse energies as low as 3 nJ.

6. Conclusions

In conclusion, light guiding in the mid-IR has been demonstrated in ULI waveguides in GASIR-1, a commercially available glass with high optical quality that transmits light up to ~15 µm. Nonlinear optical characterization has also been performed. This represents the first step in introducing GASIR-1 as a new material for ULI fabricated mid-IR integrated optics and for nonlinear optics applications. mid-IR supercontinuum generation has been shown when pumping the waveguides with femtosecond pulses centered at 4.6 µm. When pumping the largest waveguide, WG7, with 130 nJ pulses a supercontinuum spanning approximately 4 µm from 2.5 to 6.5 µm was measured. This represents the broadest and the deepest IR supercontinuum from a ULI waveguide to date. Dispersion characterization found the ZDW for WG7 to be above 4.6 µm and hence the supercontinuum was produced by pumping in the normal dispersion regime. This alludes to the possibility of even wider supercontinuum by pumping larger core GASIR-1 ULI waveguides in the anomalous dispersion regime.

Optical Materials EXPRESS

Funding

Innovation Fund Denmark (ShapeOCT, 4107-00011A); UK Engineering and Physical Sciences Research Council (CHAMP, EP/M015130/1; IDC Opt. Phot. Tech., EP/G037523/1).

Acknowledgements

The authors would like to thank the Fraunhofer Centre for Applied Photonics for their support and John Franks (Umicore N.V.) for providing the GASIR-1 samples. The work of Giorgos Demetriou was supported by a James Watt scholarship from Heriot-Watt University.